Institutionen för systemteknik
Department of Electrical Engineering

Examensarbete

Knock Detection in a Two-Stroke Engine to be Used in the Engine Management System

Examensarbete utfört i Fordonssystem
vid Tekniska högskolan vid Linköpings universitet
av

Filip Höglund

LiTH-ISY-EX--14/4744--SE

Linköping 2014

Department of Electrical Engineering
Linköpings universitet
SE-581 83 Linköping, Sweden

Linköpings tekniska högskola
Linköpings universitet
581 83 Linköping

Knock Detection in a Two-Stroke Engine to be Used in the Engine Management System

Examensarbete utfört i Fordonssystem
vid Tekniska högskolan vid Linköpings universitet
av

Filip Höglund

LiTH-ISY-EX--14/4744--SE

Handledare: **Andreas Thomasson**
            ISY, Linköpings universitet
            Henrik Eklund
            Husqvarna AB

Examinator: **Lars Eriksson**
            ISY, Linköpings universitet

Linköping, 16 februari 2014

Avdelning, Institution Division, Department Reglerteknik Department of Electrical Engineering SE-581 83 Linköping	**Datum** Date 2014-02-16

Titel Title	Knackdetektering hos tvåtaktsmotor för att användas till motorstyrningen Knock Detection in a Two-Stroke Engine to be Used in the Engine Management System
Författare Author	Filip Höglund

Sammanfattning
Abstract

Engine knock has long been a well recognized phenomenon in the automotive industry. Detecting engine knock opens up the possibility for an indirect feedback of the engine's internal combustion without installing a pressure transducer inside the cylinder. Knock detection has mainly been used for spark advance control, making it possible to control the engine close to its knock limit in search for the optimal ignition timing. This application has to a lesser extent been applied to lightweight two-stroke engines, which is the focus of this study. The investigation features a modern chainsaw engine whose knock characteristics were first determined with a pressure transducer. The structural vibrations originating from the engine knock are filtered out of the signal from a remote located accelerometer. The knock intensity is compared with the signal from the pressure transducer which shows a correlation with an accepted extent between the two sensors. Parameters that affect the knock intensity have also been investigated. These include engine temperature, different types of fuel and ignition timings.

Nyckelord Keywords	knock detection, knock control, lambda control, two-stroke engine, engine control

Abstract

Engine knock has long been a well recognized phenomenon in the automotive industry. Detecting engine knock opens up the possibility for an indirect feedback of the engine's internal combustion without installing a pressure transducer inside the cylinder. Knock detection has mainly been used for spark advance control, making it possible to control the engine close to its knock limit in search for the optimal ignition timing. This application has to a lesser extent been applied to lightweight two-stroke engines, which is the focus of this study. The investigation features a modern chainsaw engine whose knock characteristics were first determined with a pressure transducer. The structural vibrations originating from the engine knock are filtered out of the signal from a remote located accelerometer. The knock intensity is compared with the signal from the pressure transducer which shows a correlation with an accepted extent between the two sensors. Parameters that affect the knock intensity have also been investigated. These include engine temperature, different types of fuel and ignition timings.

Sammanfattning

Knack har länge varit ett välkänt fenomen inom fordonsindustrin. Att kunna detektera knack med externa sensorer öppnar upp möjligheten för en indirekt återkoppling från motorns förbränning utan att behöva montera en tryckgivare inuti cylindern. Knackdetektering har huvudsakligen använts för tändtidpunktsreglering genom att reglera motorn så nära knackgränsen som möjligt och därigenom finna en optimal tändtidpunkt. Denna applikation har inte använts lika utbrett hos lätta tvåtaktsmotorer, vilket denna studie fokuserar på. Undersökningen omfattar en modern tvåtaktsmotor vars knackkaraktäristik fastställdes genom referensmätningar med cylindertryckgivare. De strukturella vibrationerna som uppstår från knacket filtreras ut ur signalen från en avsides belägen accelerometer, och knackintensiteten jämförs med signalen från tryckgivaren. Parametrar som påverkar knackintensiteten har också undersökts, såsom motortemperatur, bränslen och tändtidpunkt.

Acknowledgments

Contents

Notation

Nomenclature	
V	Volume
B	Cylinder bore
T	Temperature
m	Mass
f	Frequency
c	Speed of sound
η	Efficiency
γ	Ratio of specific heats
λ	Air/fuel equivalence ratio

Abbreviations	
TDC	Top Dead Center
ATDC	After Top Dead Center
CAD	Crank Angle Degree
A/F	Air/Fuel
WOT	Wide Open Throttle
FFT	Fast Fourier Transform
RPS	Revolutions per Second
KI	Knock Intensity
RMS	Root Mean Square
BP	Band Pass
SNR	Signal-to-Noise Ratio

1

Introduction

1.1 Background

Today's engines have high demands on performance and emissions. The two-stroke engines used in Husqvarna chainsaws feature an electronic carburetor system called AutoTune™ which automatically compensates for different conditions such as temperature, altitude and aging. Thus, the need to manually adjust the carburetor settings as in traditional systems is not necessary. The compensation is done by leaning out the Air/Fuel mixture combusted by the chainsaw engine, and observing the change in engine speed during the lean out test. An increase in engine speed indicates that the lean out improved the output power of the engine. Consequently the AutoTune system sets the carburetor to a leaner setting. On the other hand, if the result from the lean out test shows a decrease in engine speed, the lean out test is unsuccessful and as a result the AutoTune system sets the carburetor to a richer setting, see figure 1.1.

Detecting engine knock presents a more direct feedback from the engine than the lean out and engine speed tests. A knock sensor could therefore lead to a more efficient engine management control. The intensity of the engine knock is largely dependent on the current operating condition of the chainsaw. Thus, this thesis does not only focus on how the engine knock can be detected, but also shows how the intensity of the engine knock changes with engine temperature, A/F mixture, different types of fuel and ignition timings.
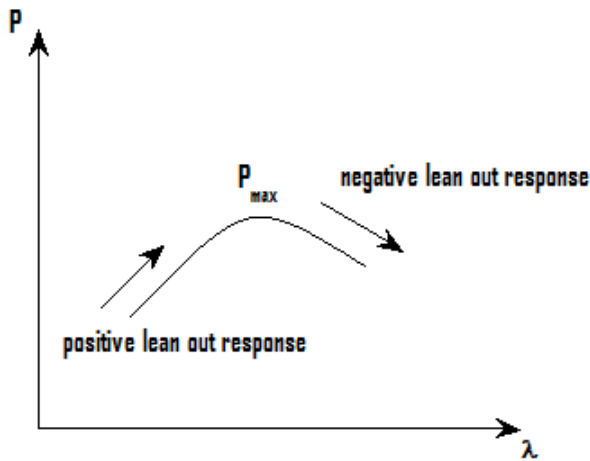
Figure 1.1: *Responses to the lean out tests from the AutoTune system. A leaner mixture corresponds to an increase in lambda, see section 2.1.*

1.2   Problem formulation

As will be explained thoroughly in section 2.3, engine knock is caused by spontaneous auto-ignitions in the end-gas region ahead of the flame front in combustion engines. Leaner A/F mixtures tend to increase the combustion temperature which increases the engine's tendency to knock.

Placing a pressure transducer inside the combustion chamber makes it possible to detect knock easily. Since this is a very expensive solution it is not suited for every single produced chainsaw. Therefore, this study investigates the performance of an accelerometer installed near the box housing the chainsaw ignition system, and the pressure transducer is used as a reference to the accelerometer. Parameters that affect the intensity of the engine knock are also investigated.

1.3   Purpose and goals

The purpose of the thesis is to investigate how the detection of engine knock in a typical Husqvarna two-stroke engine can be achieved. An analysis of similar applications made prior to the writing of the thesis has also been carried out.

The goal of the thesis is to conclude the possibilities and limitations of knock detection in a typical Husqvarna two-stroke chainsaw engine.

1.4   Related research

There has been plenty of research within the field of knock detection in four-stroke internal combustion engines. Knock detection based on accelerometers and pressure transducers has been thoroughly documented, and will be mentioned briefly in this section. Papers on knock detection in two-stroke engines are however limited.

1.4.1   Knock detection using accelerometers

The structural vibrations caused by engine knock can be detected by accelerometers, which have become widely used since they are less intrusive and easier to use than the direct measuring of cylinder pressure and ion current. Nevertheless, one disadvantage with the accelerometer is that it reacts to other moving parts in the engine, especially at higher engine speeds. Examples of interfering parts that cause vibrations are gearings, bearings and piston rings [1][2]. The higher operating engine speeds of the two-stroke engine therefore lead to heavier interfering vibrations.

The usage of wavelet-transform parameters of the accelerometer signal to enhance knock detection has been researched. It was shown that knock detection was especially improved at high engine speeds and low Signal-to-Noise ratios [3].

Installing a standard automotive accelerometer on a small 125cc four-stroke engine has proved to be possible as means of knock detection. Even a sub-optimal mounting position of the sensor yielded satisfying performance of the knock control system. This made it possible to run the engine closer to the knock limit, resulting in improved peak torque and full load fuel economy [4].

1.4.2   Knock in two-stroke engines

Investigations on parameters influencing the knock characteristics of a small, high speed two-stroke SI engine have been made in [5]. The different parameters included the air to fuel ratio, the volumetric efficiency, the engine speed and the ignition timing. The investigation included a cylinder pressure transducer together with optical probes making it possible to detect the radiation from the flame front. The probes were installed in order to determine how the flame front and knock propagate inside the cylinder.

At the standard ignition timing, around 23° before Top Dead Center (TDC), the knocking increased for leaner mixtures, higher engine speeds and lower volumetric efficiencies. The variation of the volumetric efficiency was achieved by varying the engine speed and by adjusting the exhaust back pressure at a set engine speed. When advancing the ignition timing to around 33° before TDC, the knocking was increased for leaner mixtures, higher engine speeds and higher volumetric efficiencies.

By increasing the exhaust back pressure a reduction in volumetric efficiency was achieved. This led to an increased amount of residual gas in the combustion chamber. The conclusions from the investigation are as follow:

> "The measurements have shown that for low displacement two-stroke engines, the knock intensity and the knock possibility are to a large extent dependent on the engine speed. The higher the engine speed, the higher the measured knock amplitudes and the probability of occurrence. An increase in engine speed corresponds to a decrease in volumetric efficiency and an increase in residual exhaust gas in the combustion chamber. Likewise, the volumetric efficiency, which can be varied by adjusting the exhaust backpressure, is of great importance and has a direct influence on the residual gas in the combustion chamber and on the knocking behavior. Early ignition times with a high residual gas concentration in the combustion chamber improve knocking behavior." [5].

1.5   Expected results

The expected results from Husqvarna is that detecting engine knock by using an affordable external sensor can later be used for engine management system enhancement in their two-stroke chainsaw engines. This enables the engine to be controlled more efficiently.

1.6   Thesis outline

Chapter 1 gives an introduction of the thesis by explaining its background as well as giving a short overview of similar applications in the area. Chapter 2 describes the underlying factors behind engine knock together with a simplified explanation of the two-stroke cycle. Chapter 3 introduces the reader to the experimental setup used during the thesis. Chapters 4 and 5 present the results and conclusions from the experiments.

2

Theory

The general theory behind the concepts used throughout the thesis is being described in this chapter together with an overview of the two-stroke cycle. At the end of the chapter an estimation of the combustion chamber's resonance frequency is presented. This corresponds to the detectable frequency associated with the engine knock that propagates through the engine.

2.1 The A/F equivalence ratio

The A/F equivalence ratio λ refers to an excess of air or fuel during the combustion. It is defined as the actual A/F ratio normalized with the stoichiometric A/F ratio:
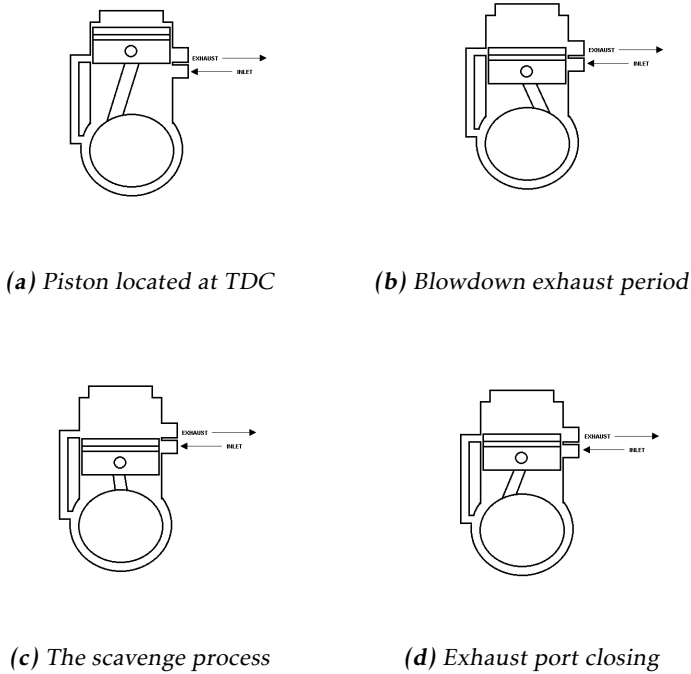
$$\lambda = \frac{(A/F)}{(A/F)_s} = \frac{(m_a/m_f)}{(m_a/m_f)_s} \tag{2.1}$$

where m_a and m_f is the mass of air and mass of fuel, respectively. The stoichiometric ratio describes the ratio between fuel and air which leaves no excess of fuel or air after combustion, see equation 2.7 for an example with iso-octane.

2.2 The two-stroke cycle

The two-stroke engine differs from its popular four-stroke counterpart in that it performs its cycle in two strokes during one crankshaft revolution, instead of four strokes during two crankshaft revolutions for the four-stroke equivalent.

5

The two-stroke engine has become widely used in lightweight power units, such as chainsaws and outboard motors due to its simplicity and high performance to weight ratio[6].

(a) Piston located at TDC   *(b)* Blowdown exhaust period

(c) The scavenge process   *(d)* Exhaust port closing

Figure 2.1: The different stages of the two-stroke cycle.

Figure 2.1 shows the different stages when filling and emptying the cylinder in a conventional two-stroke engine.

In the first stage, 2.1a, the piston is located at TDC. The compressed A/F mixture above the piston is being ignited by the spark plug. As a result there is a rise in pressure and temperature causing the piston to move downwards on the power stroke. At this stage the inlet port below the piston remains open, letting a fresh A/F mixture into the crankcase.

In the second stage, 2.1b, the exhaust port begins to open. This allows the exhaust gases out of the cylinder and into the exhaust pipe. Below the piston the fresh A/F mixture is being compressed inside the crankcase by the piston moving downwards.

In the third stage, 2.1c, the removal of exhaust gas is nearing completion and the piston has uncovered the transfer port that is connecting the cylinder with the crankcase. Due to the crankcase pressure exceeding the cylinder pressure,

the fresh A/F mixture is forced up and ultimately into the cylinder. This is the process commonly referred to as the *scavenge process* [6].

In the fourth and final stage, 2.1d, the piston is closing the exhaust port, trapping the fresh A/F mixture inside the cylinder since the transfer port is now shut. As there is no such thing as a perfect scavenge process, a small portion of the fresh A/F mixture will always leave the cylinder through the exhaust port before combustion, and some exhaust gas may still be left inside the cylinder. After the exhaust port is closed, the piston continues to compress the fresh A/F mixture until it reaches TDC and the cycle is being continued at the first stage once again.

2.2.1 Thermal efficiency

The compression ratio of the two-stroke engine is divided into two parts. The first one is the geometric compression ratio which is given by:

$$CR_g = \frac{V_{sv} + V_{cv}}{V_{cv}} \tag{2.2}$$

Where V_{sv} is the total swept volume of the engine and V_{cv} refers to the clearance volume above the piston when located at TDC, i.e. the volume of the combustion chamber. This is the compression ratio usually referred to in the case of four-stroke engines.

The second part is the trapped compression ratio and is given by:

$$CR_t = \frac{V_{ts} + V_{cv}}{V_{cv}} \tag{2.3}$$

Where V_{ts} is the swept volume after the exhaust port has been closed.

The thermal efficiency of the two-stroke engine is approximated as [6]:

$$\eta_t = 1 - \frac{1}{CR_t^{\gamma-1}} \tag{2.4}$$

where γ is the ratio of specific heats. This efficiency does not take any losses due to friction, heat transfer etc. into account. As can be seen, the thermal efficiency for the ideal engine is only dependent on one design parameter. This parameter is mainly limited due to a phenomenon called *engine knock*.

2.3 Knock fundamentals

Knock is the resonance phenomenon caused by spontaneous auto-ignition in the end-gas region ahead of the flame front in a combustion engine. The end-gas region contains the unburned A/F mixture which the spark-ignited flame kernel propagates through until it is extinguished at the cylinder walls. Due to the high local pressure increase, a pressure wave begins to propagate across the combustion chamber, which in turn causes the chamber to resonate at its natural frequencies [7].
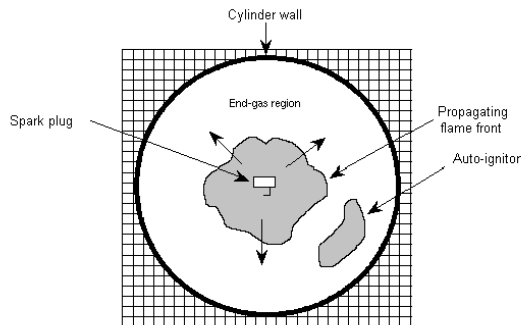
Figure 2.2: *The propagating flame front together with an auto-ignition seen from above the cylinder.*

There are different theories explaining the occurrence of knock. The auto-ignition theory states that the high temperature and pressure in the end-gas region cause auto-ignition, see figure 2.2. The detonation theory suggests that when the flame-front accelerates to supersonic velocities, the corresponding shock wave causes the end-gas to self ignite.

Knock sets the limit for the possible compression ratio of the engine, and therefore also its performance and efficiency, see (2.4).

2.3.1 Knock detection

Detecting knock is mainly done with three different methods. These methods utilize the cylinder pressure, ion current measurements inside the combustion chamber and accelerometers.

Knock can be easily distinguished from the cylinder pressure trace, see figure 2.3. Pressure transducers, however, are mostly used in research engines due to their high cost.

(a) *Pressure trace with heavy knock*

(b) *Pressure trace with no knock*
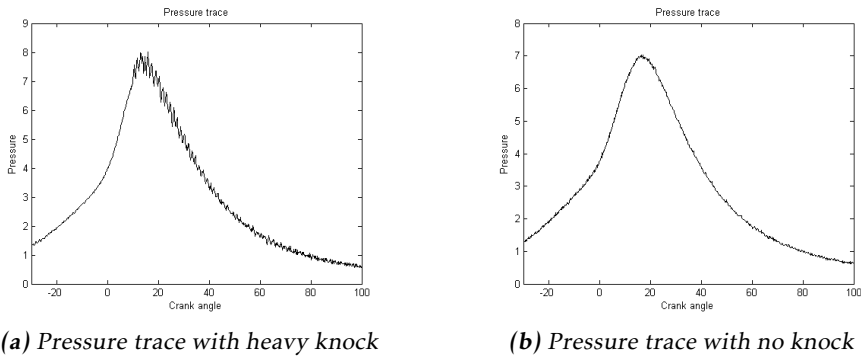
Figure 2.3: *Difference between a knocking and a non knocking cycle.*

The ionic current inside the combustion chamber is measured by applying a sense voltage between the electrodes of the spark plug when it is not used for firing. The sensed current is dependent on the concentration of ions which are created by the chemical reactions in the flame front. The sensed current is connected to the cylinder pressure and to the oscillations seen around the pressure peak in figure 2.3a. The sensed current can therefore be filtered around the knock frequency and used as knock detection [7].

2.3.2 Knock control

The engine's tendency to knock is largely dependent on parameters deciding the temperature and pressure of the end-gas during combustion [8]. Another important parameter is the fuel's resistance to knock which is measured by its octane number. This is dependent on the chemical structure of the fuel. Fuels with higher octane numbers have higher antiknock qualities.

Furthermore, knock is prevented by varying the ignition timing. A later ignition leads to lower end-gas temperatures. Retarding the ignition from its optimal timing, however, results in lower output torque. It is therefore essential to control the engine as close to the knocking limit as possible, without causing damage to the engine.

2.4 Estimation of resonance frequency

The frequency of the resonances caused by engine knock is coupled with the geometry of the combustion chamber and the speed of sound inside the cylinder. The frequency is composed of three different components, namely a circumferential, a radial and an axial mode. Assuming that the combustion chamber is a perfect cylinder with flat ends, the resonance frequencies are given by Draper's equation [9]:

$$f_{n,m,p} = \alpha_{n,m,p} \frac{c}{\pi B} \tag{2.5}$$

where c denotes the speed of sound in the gas, B the cylinder bore diameter and the indices n, m and p are integers denoting the circumferential, radial and axial mode numbers. These mode numbers are determined by the Bessel Equation, and the three first circumferential mode numbers and the first radial mode number are presented in table 2.1. The first circumferential mode is the first mode to be excited, the frequency of which creates the typical "pinging" sound associated with knock [10].

Mode	$\alpha_{n,m,p}$
1,0,0	1.841
2,0,0	3.054
0,1,0	3.832
3,0,0	4.201

Table 2.1: Mode numbers for different resonance modes. Taken from [11].

The speed of sound in the exhaust gas is difficult to estimate but can be calculated assuming an ideal gas (2.6) from a stoichiometric combustion of iso-octane (2.7).

The speed of sound in an ideal gas is given by:

$$c = \sqrt{\frac{\gamma k T}{m}} \tag{2.6}$$

where γ is the ratio of specific heats, k is the Boltzmann constant, m is the molecular mass of the gas and T is the mean temperature in K of the gas during combustion.

A stoichiometric combustion reaction between iso-octane $C_8 H_{18}$ and air which only results in water and carbon dioxide gives an approximation of the molecular mass m. This stoichiometric combustion is given by [7]:

$$C_8 H_{18} + 12.5 O_2 + 12.5 \cdot 3.773 N_2 \rightarrow 8 CO_2 + 9 H_2 O + 12.5 \cdot 3.773 N_2 \tag{2.7}$$

Assuming a mean temperature of 1800°C during combustion, the speed of sound can at this stage be calculated to about 920 m/s.

The first resonance frequency can now be calculated using (2.5) and a cylinder bore of 46 mm:

$$f_{1,0,0} = 1.841 \frac{920}{\pi \cdot 0.046} \approx 12 \text{ kHz} \tag{2.8}$$

Which shows that the expected resonance frequency of the small 2-stroke engine is significantly higher than that of a typical automotive engine, whose first resonance frequency often lies around 6 kHz. A frequency close to which most knock sensors are developed to detect [10].

3

System description

This chapter gives an overview of the chainsaw engine and measurement equipment used during the thesis. A phenomenon that affected the measurements from the cylinder pressure transducer is also depicted. This phenomenon happened because of the mounting technique involved in connecting the sensor with the combustion chamber.

3.1 Engine specifications

The Husqvarna 560 XP® chainsaw model features a single cylinder air cooled two-stroke engine, see engine specifications in table 3.1. The carburetor that supplies the engine with the A/F mixture uses the AutoTune™ system, which automatically adjusts the A/F ratio depending on different parameters, see section 1.1.

Bore	46 mm
Stroke	36 mm
Cylinder displacement	60 cm^3
Geometric compression ratio	10.5:1
Power output	3.5 kW
Maximum power speed	9600 rpm
Idling speed	2800 rpm
Maximum torque	3.65 Nm @ 8100 rpm

Table 3.1: Engine specifications

3.2   Sensors

3.2.1   Cylinder pressure transducer

The cylinder pressure has been measured using a Kistler 6052C72 cylinder pressure transducer [12], which consists of a piezoelectric crystal that generates an electric charge when subjected to a mechanical load. The sensor is coupled with a charge amplifier to convert the electrical charge into an amplified voltage signal which can later be processed and analyzed. The sensor has a very high natural frequency around 160 kHz, making it suitable for knock detection. This sensor is used as a reference to the other alternative.

3.2.2   Accelerometer

The accelerometer used to measure the vibrations originating from the knock is a miniature piezoelectric accelerometer model no. 352A21 [13] manufactured by PCB Piezotronics. With a frequency range up to 20kHz and a natural frequency greater than 50 kHz, it is suited to detect the first resonance frequency. The sensor uses a built-in charge-to-voltage converter that requires an excitation voltage. It is therefore connected to a signal conditioner that feeds the correct excitation voltage to the accelerometer.

The placement of the accelerometer is chosen close to the ignition system seen in figure 3.1, keeping in mind that a permanent installation of an accelerometer at this location is advantageous due to cabling and other costs.
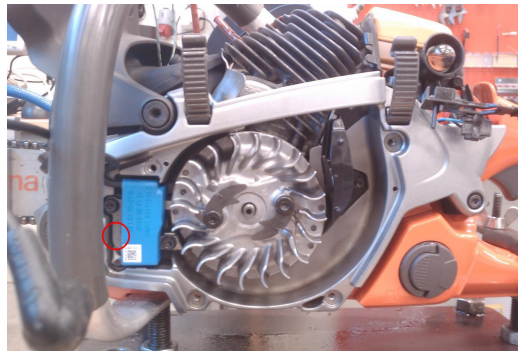
Figure 3.1: *The ignition system is the blue box at the side of the fan wheel. The accelerometer is placed on top of the iron core going through the ignition system. The two bolts keeping the iron core bolted to the crankcase can also be seen.*

However, as can be seen in figure 3.1, the possible space for installing an accelerometer at this location is limited. The width of the accelerometer is 6.4 mm, making it possible to glue it onto the iron core with a temperature resistant adhesive. Usually knock sensors of this kind are placed closer to the combustion chamber in order to decrease vibration attenuation. The iron core is bolted to the crankcase and the acceleromter is therefore in contact with the vibrations coming from the combustion chamber. The adhesive mounting technique of the sensor is not expected to affect the sensitivity deviation in the frequency range close to the first resonance frequency of the engine knock.

3.3   Auxiliary units

A National Instruments USB 6356 [14] was used for the data acquisition of the sensors with a sampling frequency equivalent to 5 samples per Crank Angle Degree (CAD). This makes the sampling frequency dependent on the engine speed, which was found not to vary significantly during the crankshaft revolution. To assort the correct CAD to each sample an index pulse from the ignition system was used. The index pulse begins at a fixed CAD for each crankshaft revolution. This index pulse was acquired together with the other sensors.

3.4   Experimental procedure

The engine was connected to a dynamometer via the drive shaft. The dynamo is able to adjust the output torque which enables the engine to be run at a constant engine speed for the whole data acquisition period. The engine was let to run at Wide Open Throttle (WOT) until reaching the desired lambda value and the data was then sampled under stable engine conditions.

3.5   Pressure oscillations

As illustrated in figure 3.3 below, the unprocessed cylinder pressure signal still contains high frequency oscillations far from the pressure peak. These oscillations stem from the recess in which the cylinder pressure transducer has been installed. As the transducer could not be flush mounted, i.e in direct contact with the combustion chamber, a standing wave phenomenon inside the duct caused unwanted oscillations in the pressure signal.
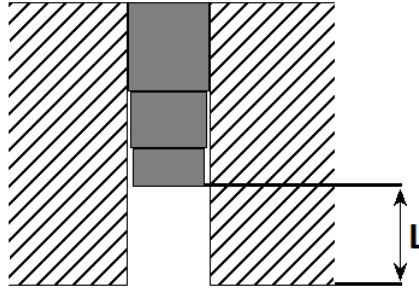
Figure 3.2: *The duct in which the pressure sensor was mounted. The sensor head is L mm away from the combustion chamber.*
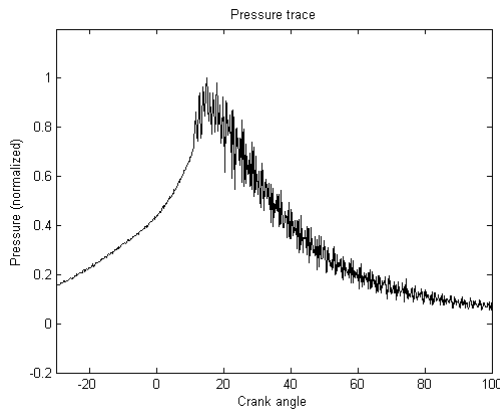
Figure 3.3: *Pressure trace showing the high frequencies stemming from the recess mounting of the pressure transducer.*

The first harmonic of the standing wave in the duct can be calculated as follows:

$$f = \frac{c}{4L} \tag{3.1}$$

where f is the first harmonic frequency of the duct, c the same speed of sound as in 2.5 and L the length of the duct.

The shortest possible duct length for the chainsaw header is 2.5 mm. By using the same speed of sound as in section 2.4 the harmonic frequency of the duct is found to be around 90 kHz. The pressure signal is therefore low-pass filtered to remove these high frequencies from the knock frequencies in the later signal processing, see figure 3.4.

(a) *Pressure trace without low-pass filter.*

(b) *Low-pass filtered pressure trace.*
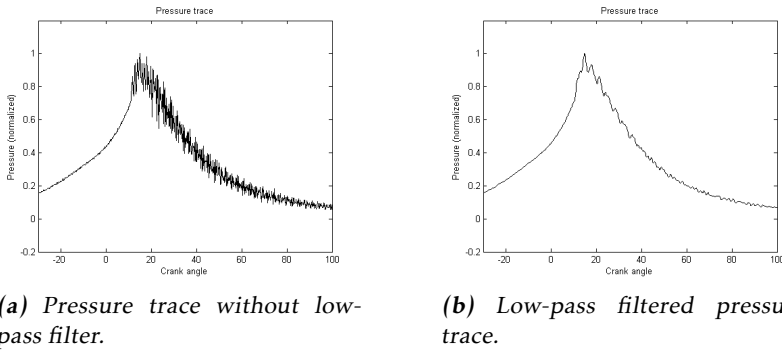
Figure 3.4: *The difference of a pressure cycle after low-pass filtering.*

This phenomenon is later confirmed with measurements from a duct length of 20 mm. The pressure trace now shows a dominant frequency at around 10 kHz, which is expected from equation 3.1.

(a) *Pressure trace from a duct length of 20 mm.*

(b) *FFT for the same pressure trace. Peak at 10 kHz.*
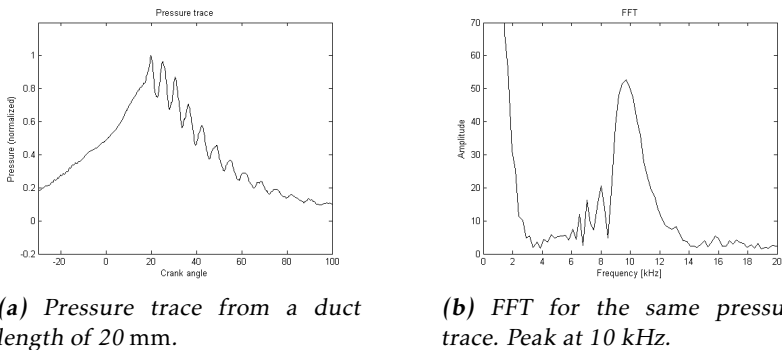
Figure 3.5: *Pressure trace and FFT for a longer duct length.*

Studies concerning this phenomenon have been done prior to this thesis. In paper [15] the measured frequencies were also found to be very close to the approximated frequency from equation 3.1.

4

Signal processing

The aim of this chapter is to give an overview of the methods used for data processing as well as analyzed and interpreted results. Firstly the pressure signal is processed to give an understanding about what to look for in the accelerometer signal. Secondly the accelerometer signal is processed and compared to the pressure signal.

Power spectrum of the collected sensor data has been done using the *fft* command in MATLAB which is included in the Signal Processing Toolbox. This enables the frequencies in the different signals to be easily interpreted.

4.1 Knock frequencies in the pressure signal

Figures 4.1 to 4.3 show the power spectrum of the pressure signals under three different engine conditions. Each series of data consists of approximatively 110 consecutive pressure cycles. All in all, four peaks can be seen in all of the power spectrums. Three of these peaks have the same order of magnitude as the frequencies found in section 2.4. The first is around 16 kHz, the second at 32 kHz and the third just above 40 kHz. The second frequency is closer to the third frequency than the first frequency which matches the resonance mode numbers in table 2.1. The amplitude of these frequencies increases for leaner A/F mixtures, which is to be expected since leaner mixtures increase the engine's tendency to knock as well as the knock intensity. Since the combustion chamber is not a perfect cylinder but hemispherical a perfect match with the frequencies found in section 2.4 can not be expected. The frequencies above 20 kHz are unfeasible to detect with the accelerometer in question. Therefore the first resonance frequency at 16 kHz will be the main focus in the later signal processing.
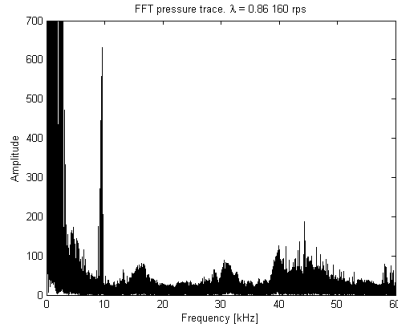
Figure 4.1: *FFT for unfiltered pressure data series collected at lambda 0.86 and 160 rps*
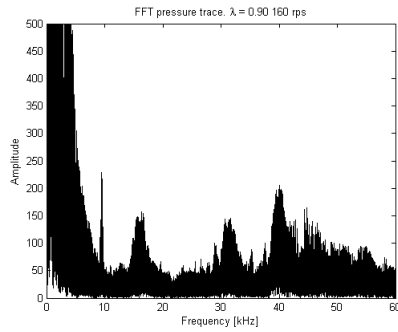

Figure 4.2: *FFT for unfiltered pressure data series collected at lambda 0.90 and 160 rps.*
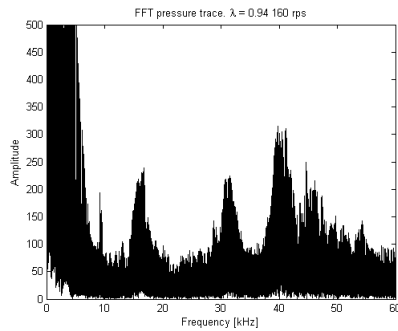
**Figure 4.3:** *FFT for unfiltered pressure data series collected at lambda 0.94 and 160 rps*

4.1.1   The frequency not associated with engine knock

The peak at around 9 kHz does not seem to increase in amplitude with leaner A/F mixtures. A zoomed in version of the FFT in figure 4.1 around this peak shows that it actually consists of multiple peaks spaced apart by an even multiple of the engine speed, which is 160 rps.
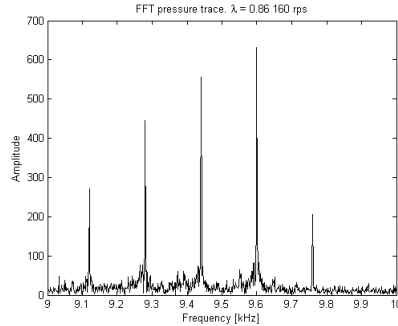
Figure 4.4: *Zoomed in FFT at the peak around 9 kHz*

It is hard to determine what causes these peaks. Nevertheless, the MATLAB command *spectrogram* in figure 4.5 enables a time-frequency diagram of the pressure signal to be analyzed.
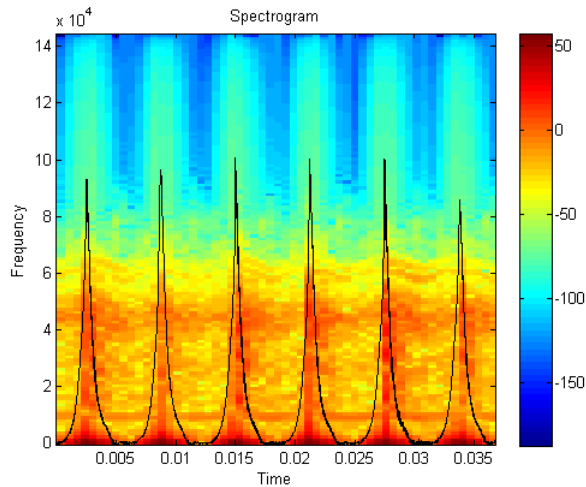
Figure 4.5: *Time-frequency content of six consecutive pressure cycles. Note the frequency band at around 9 kHz that is present during the whole crank shaft revolution. Low-pass filtered at 60 kHz.*

The *spectrogram* command divides the signal into different segments with a specified sample length. The FFT of each segment is computed and the result is plotted in a time-frequency diagram. The amplitude of the FFT:s is translated into colours and can be seen as vertical lines in the spectrogram. In figure 4.5 six consecutive pressure cycles have been used in the spectrogram, and the pressure traces are plotted on top of the spectrogram to make the interpretation easier.

The frequency around 9 kHz found in the FFT:s on page 20 can be distinguished as a horizontal line through the whole spectrogram. This frequency is therefore not connected to engine knock alone, and will not be used when filtering out knock frequencies in further signal processing. Energy content above 40 kHz also seems to be present in the whole spectrogram. The filtering is therefore done using a narrow Band Pass (BP) filter around the first resonance frequency to avoid this frequency content.

Figure 4.6 confirms that the three other peaks on page 20 appear around the expected occurrence of knock in the pressure trace. It also confirms that the peak at around 9 kHz can not be associated with engine knock.
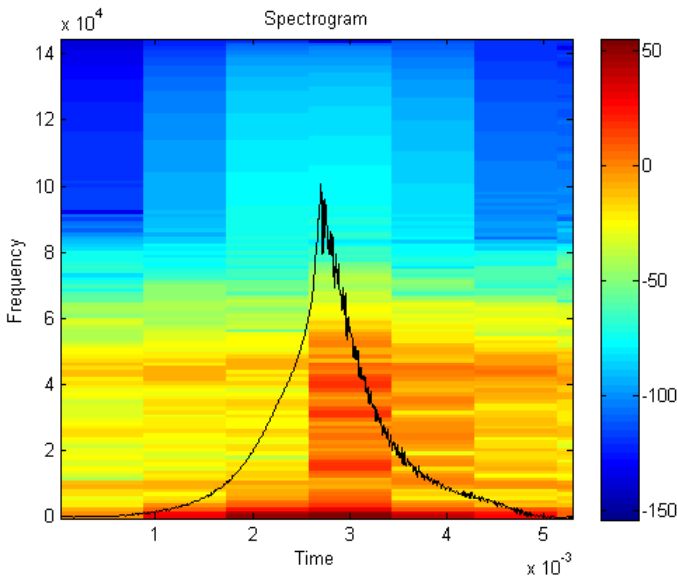
Figure 4.6: *Spectrogram of a single pressure cycle. Note the three frequency bands at around 16, 32 and 40 kHz just after the pressure peak. Low-pass filtered at 60 kHz.*

4.1.2   Knock onset

Instead of analyzing entire sensor signals a small portion of the signal is selected and analyzed. This portion of the signal will henceforth be referred to as "knock window". In order to determine this window each pressure trace is high-pass filtered. The knock onset is defined as the first peak in the high-pass filtered signal exceeding a certain threshold, see figure 4.7.
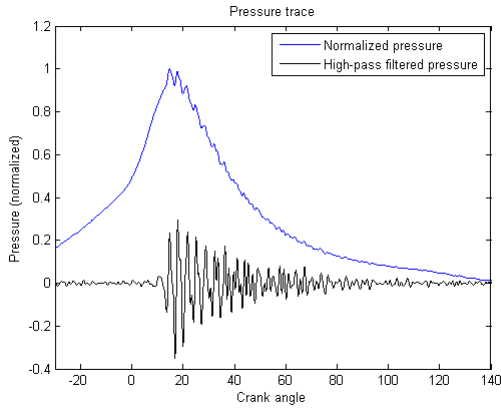
Figure 4.7: *Pressure trace together with 12 kHz high-pass filtered pressure signal. The threshold for knock onset is set to 0.05. Here knock onset is just before 20 CAD ATDC.*

Figure 4.8 shows the distribution of the knock onset for four different engine operating conditions running at WOT.
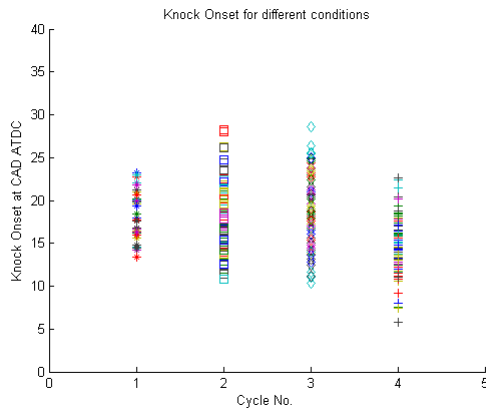
Figure 4.8: *Distribution of knock onset for various engine operating conditions. See table 4.1 for the operating condition of each cycle.*

Cycle No.	Engine speed [rps]	λ
1	140	0.86
2	160	0.80
3	160	0.86
4	160	0.90

Table 4.1: Engine operating conditions.

Knock for most cycles usually begins around 20 CAD ATDC. Knock seems to start somewhat earlier for very lean mixtures, i.e. heavy knocking cycles. It is difficult to determine at which CAD the knock ends as the high-pass filtered signal in 4.7 still contains background noise after the knock has ended. Closer observations of the pressure traces reveal that a knock window between TDC and 50 CAD ATDC is well suited for the pressure transducer signals.

4.1.3   Knock intensity evaluation

In order to remove as much background noise as possible the pressure signal was BP filtered around the first resonance frequency just below 16 kHz. The BP filter used in this study is a 5'th order Butterworth filter with a cut-off frequency of 14.5 - 16.5 kHz. The filtering of data was done using the *filtfilt* command in MATLAB which filters the input data in both the forward and reverse direction, resulting in a doubling of the filter order. The resulting filter order is important since larger filter orders give shorter transition bands, but also longer impulse responses and larger group delays [16]. The result from BP filtering a pressure trace with the chosen filter can be seen in figure 4.9
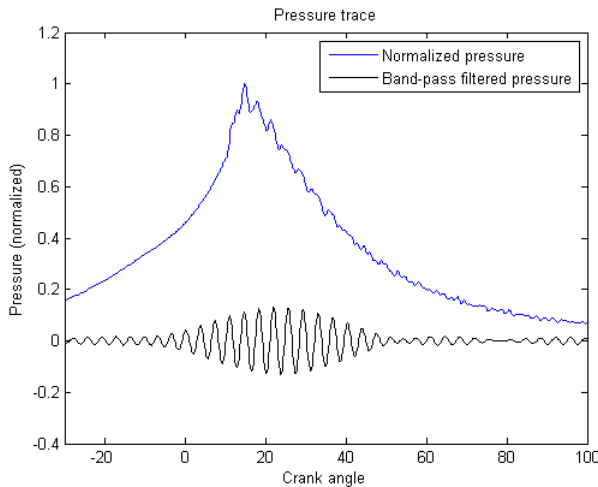
Figure 4.9: Pressure trace together with BP filtered pressure signal with a cut-off frequency of 14.5 - 16.5 KHz. Acquired at lambda 0.86 and 160 rps

Now the BP filtered data can be used for knock intensity evaluation by computing knock intensities for each cycle. The two intensities focused on in this study are widely used in similar applications and can easily be compared with intensities computed from other operating conditions and sensors.

The first knock intensity is defined as the maximum amplitude of the BP filtered data. The second intensity is the Root Mean Square (RMS) of the same data. These can also be stated as:

$$KI_{amp} = \max\left(X_1, X_2, ..., X_n\right) \tag{4.1}$$

$$KI_{RMS} = \sqrt{\frac{1}{n}(X_1^2 + X_2^2 + ... + X_n^2)} \tag{4.2}$$

where the vector X_i , $i = 1, ..., n$ contains the samples from the BP filtered data inside the knock window. This means that sample X_1 corresponds to the first sample after the piston has passed TDC, and sample X_n corresponds to the last sample before the crankshaft has rotated to 50 CAD ATDC.
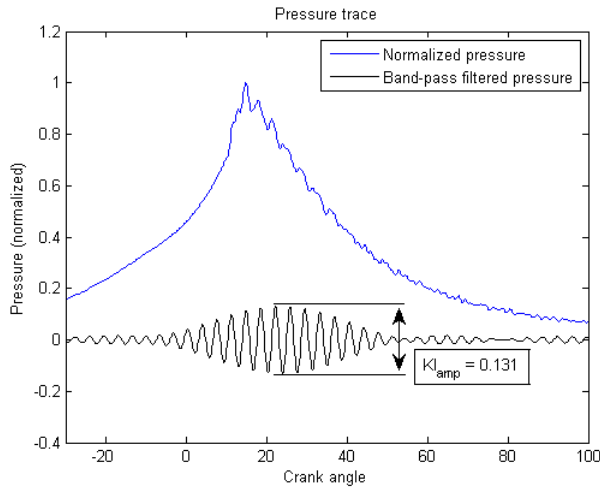
Figure 4.10: *Pressure trace and computed KI using equation 4.1. For this pressure cycle equation 4.1 is equals 0.131. Acquired at lambda 0.90 and 160 rps*
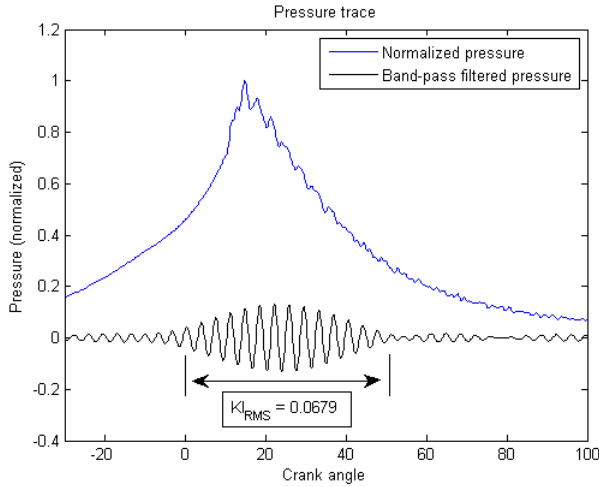
Figure 4.11: *Pressure trace and computed KI using equation 4.2. For this pressure cycle equation 4.2 is equals 0.0679. Acquired at lambda 0.90 and 160 rps*

Figure 4.10 and 4.11 show two examples of computed KI. As can be seen, KI_{amp} is only dependent on the maximum amplitude of the filtered pressure, whereas KI_{RMS} computes knock intensity using every sample inside the knock window.

The results from computing the same KI:s for each cycle under different engine operating conditions can be seen in table 4.2. The acquired data for each lambda measurement consists of approximatively 110 consecutive pressure cycles with the same engine speed.

λ	$\overline{KI_{amp}}$	max KI_{amp}	$\overline{KI_{RMS}}$	max KI_{RMS}
0.86	0.0285	0.1463	0.0147	0.0751
0.90	0.0599	0.2434	0.0310	0.1243
0.94	0.0844	0.3909	0.0436	0.2026

Table 4.2: *Knock intensities for different A/F ratios. The cells contain the mean and maximum intensities computed from about 110 consecutive pressure cycles. Knock intensity increases for leaner A/F mixtures.*

The mean and maximum value for both KI:s are nearly three times higher when comparing lambda 0.94 to lambda 0.86. There is a strong correlation between knock intensity and leaner A/F mixtures. However, as previously stated in section 2.3.1, pressure transducers are way too expensive to be a permanent solution.

4.2   Knock frequencies in the accelerometer signal

Plotting power spectrum for the unfiltered accelerometer signal does not reveal any immediate predominant frequencies. Some disturbances from the ignition system can also be seen in the unfiltered signal. Assuming that the frequency has not changed much compared to the first frequency found in the cylinder pressure trace, the accelerometer signal can be BP filtered using the same filter as in section 4.1.3.

An example of a BP filtered accelerometer signal together with the corresponding pressure trace for easier interpretation can be seen in figure 4.12.
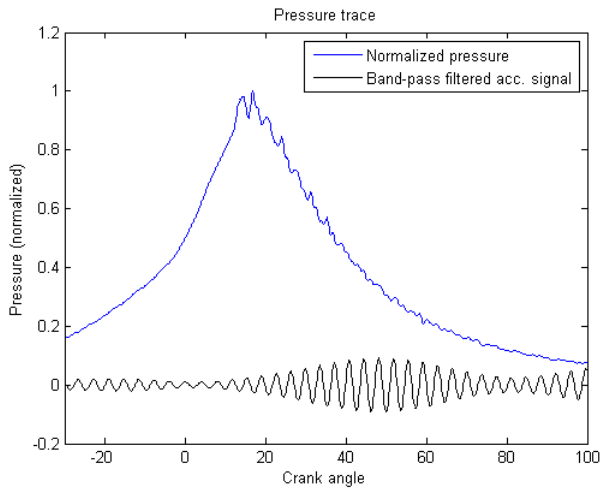
Figure 4.12: *Pressure trace and BP filtered accelerometer signal using the same cut-off frequency as with the pressure signal. Knock window seemingly between 20 and 80 CAD ATDC. Acquired at lambda 0.86 and 160 rps*

As can be seen the knock is somewhat delayed because of the accelerometer being placed farther away from the cylinder, see section 3.2.2. It is difficult to determine knock onset similarly to that of the pressure transducer. After analyzing multiple pressure traces like the one in figure 4.12, a knock window between 20 and 80 CAD ATDC was found to be adequate for computing KI:s.

Since the placement and mounting technique of the accelerometer lead to vibration attenuation together with other noise sources the best cut-off frequency of the BP filter may differ from the one used in the pressure signal. The SNR has been examined for different BP filters in order to find a suiting filter cut-off frequency for the accelerometer signal.

4.2.1   BP filtering the accelerometer signal

The choice of cut-off frequency for the BP filter was based upon the SNR using a heavy knocking cycle and a non-knocking cycle:

$$SNR = 20 * log \frac{A_{signal}}{A_{noise}} = 20 * log \frac{KI_{RMS,heavy\ knock}}{KI_{RMS,no\ knock}} \ [dB] \qquad (4.3)$$

SNR usually compares the amount of wanted signal to the amount of unwanted background noise. In this case it becomes the ratio of the accelerometer signal between a knocking and a non-knocking cycle. To measure this it is convenient to use the already defined knock intensities. Therefore the KI:s in equation 4.3 are defined similarly as in section 4.1.3 but computed during the different knock window. This is also somewhat similar to what a future implementation of knock control in a produced engine may look like.

The SNR is computed for four different cut-off frequencies, making the BP filter narrower and narrower around the knock frequency found in the pressure signal. The two pressure cycles and the corresponding unfiltered accelerometer signal for three different engine operating conditions used to compute SNR can be seen in figure 4.13 to 4.15
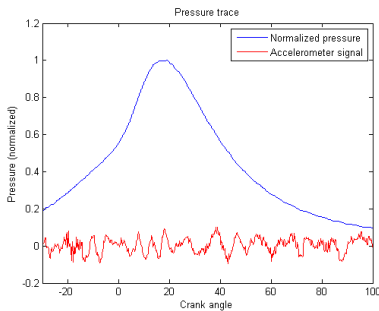
(a) Accelerometer signal in red. **Non-knocking** cycle means that the computed KI from this cycle will be used as **noise** in equation 4.3
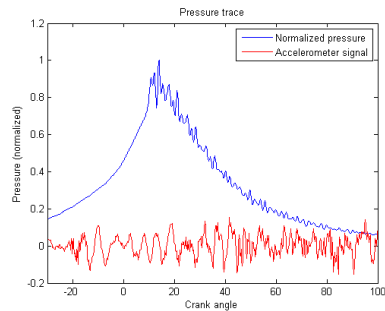
(b) Accelerometer signal in red. **Heavy knocking** cycle means that the computed KI from this cycle will be used as **signal** in equation 4.3

Figure 4.13: Non-knocking and heavy knocking cycle. Unfiltered accelerometer signal in red. Acquired at lambda 0.80 and 160 rps.
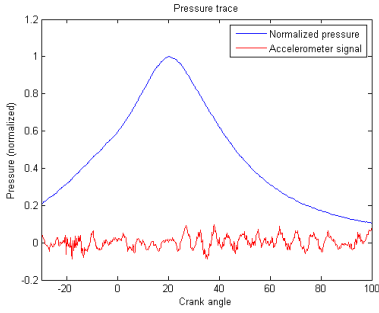
(a) *Accelerometer signal in red.* **Non-knocking** *cycle means that the computed KI from this cycle will be used as* **noise** *in equation 4.3*
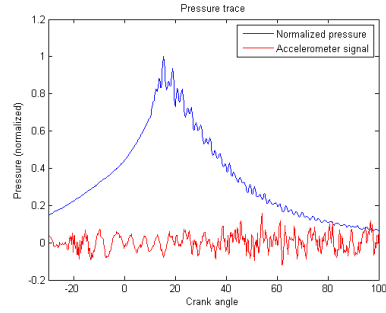
(b) *Accelerometer signal in red.* **Heavy knocking** *cycle means that the computed KI from this cycle will be used as* **signal** *in equation 4.3*

Figure 4.14: *Non-knocking and heavy knocking cycle. Unfiltered accelerometer signal in red. Acquired at lambda 0.83 and 160 rps.*
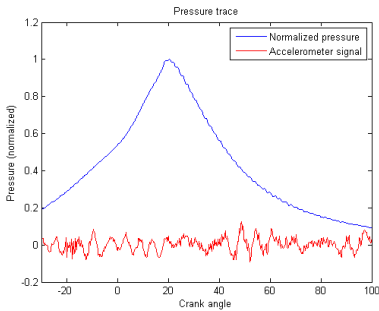
(a) *Accelerometer signal in red.* **Non-knocking** *cycle means that the computed KI from this cycle will be used as* **noise** *in equation 4.3*
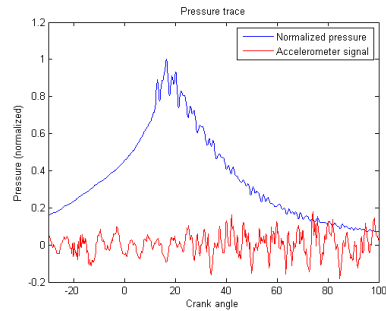
(b) *Accelerometer signal in red.* **Heavy knocking** *cycle means that the computed KI from this cycle will be used as* **signal** *in equation 4.3*

Figure 4.15: *Non-knocking and heavy knocking cycle. Unfiltered accelerometer signal in red. Acquired at lambda 0.90 and 160 rps.*

The disturbance from the ignition system due to the index pulse can be seen at around 20 CAD before TDC in the red line. It does not affect the signal during the occurrence of knock since the vibrations arrive at the accelerometer around 20 CAD ATDC.

The four different BP filters are now applied to each of the accelerometer signals in the above figures. The resulting SNR:s are presented in table 4.3 to 4.5.

BP cut-off frequency	Signal-Noise-Ratio [dB]
12.5 - 18.5 kHz	18.16
13.5 - 17.5 kHz	21.46
14.5 - 16.5 kHz	32.43
14.8 - 16.2 kHz	33.08

Table 4.3: *SNR for different cut-off frequencies. Computed for data acquired at lambda 0.80 and 160 rps.*

BP cut-off frequency	Signal-Noise-Ratio [dB]
12.5 - 18.5 kHz	22.69
13.5 - 17.5 kHz	26.27
14.5 - 16.5 kHz	32.94
14.8 - 16.2 kHz	29.09

Table 4.4: *SNR for different cut-off frequencies. Computed for data acquired at lambda 0.83 and 160 rps.*

BP cut-off frequency	Signal-Noise-Ratio [dB]
12.5 - 18.5 kHz	26.05
13.5 - 17.5 kHz	30.81
14.5 - 16.5 kHz	50.27
14.8 - 16.2 kHz	57.31

Table 4.5: *SNR for different cut-off frequencies. Computed for data acquired at lambda 0.90 and 160 rps.*

First of all the SNR is higher with leaner mixtures due to the signal portion being higher for heavier knock cycles. The most narrow BP filter tends to have the highest SNR. This is not the case in table 4.4, but it is close to the somewhat broader BP filter in the cell above.

In conclusion a BP filter cut-off frequency of 14.5 - 16.5 kHz leads to satisfying performance and will be used for the accelerometer signal, making it the same as the BP filter used for the pressure signal.

4.2.2   Accelerometer and pressure transducer cross-correlation

After BP filtering and computing KI:s for the accelerometer signal the result can be compared with the KI:s from the pressure transducer. To make the comparison easier each KI from both sensors is normalized, i.e divided by the maximum computed KI from each sensor. This means that a KI whose value equals 1.0 corresponds to the heaviest knocking cycle in the series. The KI:s from the accelerometer and pressure transducer are then plotted against each other, and the corresponding cross-correlation is also computed. Each data series consists of 400 consecutive pressure cycles, which in turn corresponds to 400 computed KI:s from both the pressure transducer and accelerometer.

(a) KI_{amp} *(b)* KI_{RMS}
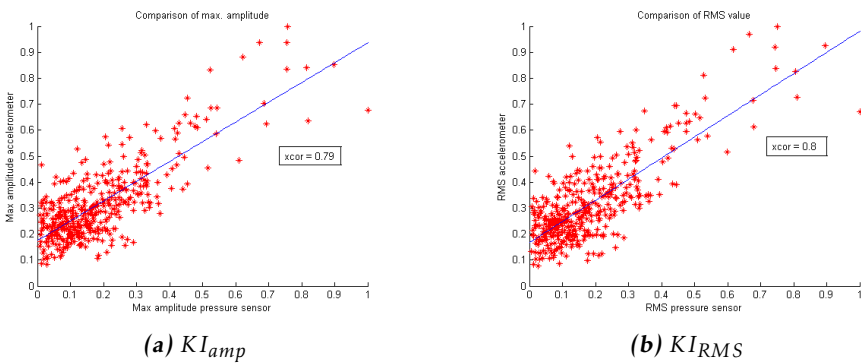
Figure 4.16: *Cross correlation of knock intensities from accelerometer and pressure signals. Acquired at lambda 0.80 and 160 rps.*

(a) KI_{amp} *(b)* KI_{RMS}
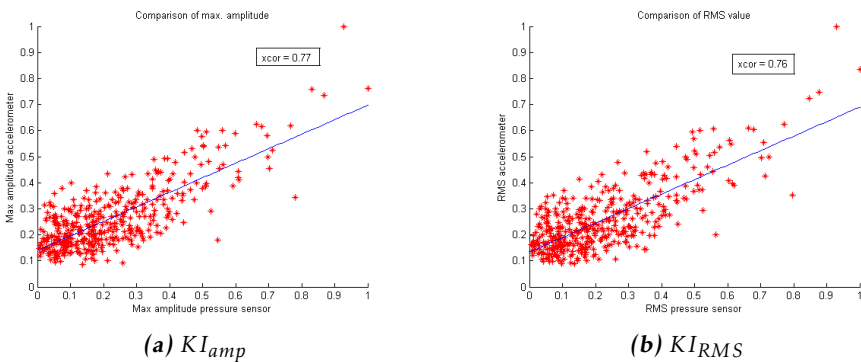
Figure 4.17: *Cross correlation of knock intensities from accelerometer and pressure signals. Acquired at lambda 0.83 and 160 rps.*

(a) KI_{amp}

(b) KI_{RMS}
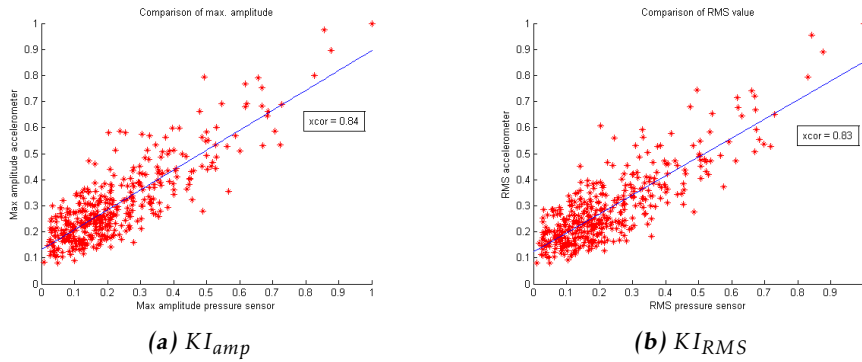
Figure 4.18: *Cross correlation of knock intensities from accelerometer and pressure signals. Acquired at lambda 0.90 and 160 rps.*

The KI:s from the accelerometer correlate to an accepted extent with the KI:s from the pressure transducer. The accelerometer is rather good at sensing non-knocking and heavy knocking cycles. On the other hand it is inadequate sensing light, medium and fairly heavy knocking cycles correctly. The best correlated KI:s are from the leanest data series in figure 4.18, which contains the heaviest knocking cycles of the three data series. Since this method of detecting knock is commonly used, the problem may be that the accelerometer is mounted too far away from the source of engine knock. This together with the very high engine speed of the two-stroke engine make the background noise significantly higher than usual when using accelerometers as knock detectors.

The KI:s for non-knocking cycles are also higher than the KI:s from the pressure transducer due to the higher background noise in the accelerometer signal. This leads to the offset seen in the vertical axis in the above figures.

To test different accelerometer placements is difficult since the operating range of the sensor is limited to +120°C and the temperature at the top of the cylinder block is close to +250°C. The temperature farther down the cylinder block is not as high, but there is still a risk for the accelerometer to overheat. It is also essential that the accelerometer is installed on top of a flat surface in order to function properly. The accelerometer is also air cooled directly by the rotating fan wheel seen in figure 3.1 when mounted close to the ignition system.

4.3   Knock intensity dependency on engine temperature

So far the engine knock has been measured after the engine has been warmed up and has reached a stable temperature. This is not the case during a normal operation of a chainsaw. It is therefore interesting to see how the knock intensity varies with different engine temperatures. The engine was first warmed up to a stable engine temperature, and then let to run at idle until the cylinder was cooled to about +150°C. After being cooled down the engine was run at WOT and the pressure was measured for three different cylinder temperatures corresponding to the temperature range during a normal chainsaw operation. See the temperatures in table 4.6.

Temperature	°C
T1	175
T2	210
T3	~ 250

Table 4.6: *The three different engine temperatures during pressure measurements.*

The resulting KI:s from the pressure measurements can be seen in table 4.7 to 4.9. The cells contain the mean and maximum intensities computed from 400 consecutive pressure cycles. These KI:s were computed the same way as they were in section 4.1.3. To see the pressure traces that these KI:s correspond to, see appendix A.1.

λ	Temperature	$\overline{\mathrm{KI_{amp}}}$	max $\mathrm{KI_{amp}}$	$\overline{\mathrm{KI}}$	max $\mathrm{KI_{RMS}}$
0.80	T1	0.0044	0.0331	0.0023	0.0170
0.80	T2	0.0092	0.0702	0.0048	0.0357
0.80	T3	0.0400	0.2110	0.0200	0.1100

Table 4.7: *Knock intensities for different engine temperatures. Acquired at lambda 0.80 and 160 rps.*

λ	Temperature	$\overline{\mathrm{KI_{amp}}}$	max $\mathrm{KI_{amp}}$	$\overline{\mathrm{KI_{RMS}}}$	max $\mathrm{KI_{RMS}}$
0.90	T1	0.0059	0.0609	0.0030	0.0310
0.90	T2	0.0158	0.1060	0.0081	0.0544
0.90	T3	0.0581	0.2582	0.0298	0.1326

Table 4.8: *Knock intensities for different engine temperatures. Acquired at lambda 0.90 and 160 rps.*

λ	Temperature	$\overline{\mathrm{KI_{amp}}}$	max $\mathrm{KI_{amp}}$	$\overline{\mathrm{KI_{RMS}}}$	max $\mathrm{KI_{RMS}}$
0.94	T1	0.0071	0.0687	0.0036	0.0349
0.94	T2	0.0215	0.1184	0.0109	0.0605

Table 4.9: *Knock intensities for different engine temperatures. Acquired at lambda 0.94 and 160 rps.*

(a) $\overline{KI_{amp}}$ ***(b)*** $\overline{KI_{RMS}}$
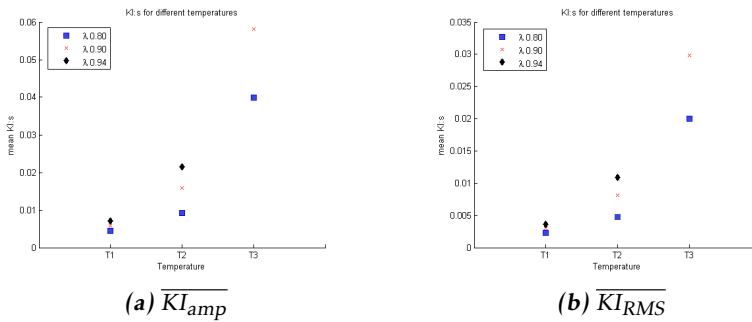
Figure 4.19: *Scatter plot for mean KI:s.*

(a) max KI_{amp} ***(b)*** max KI_{RMS}
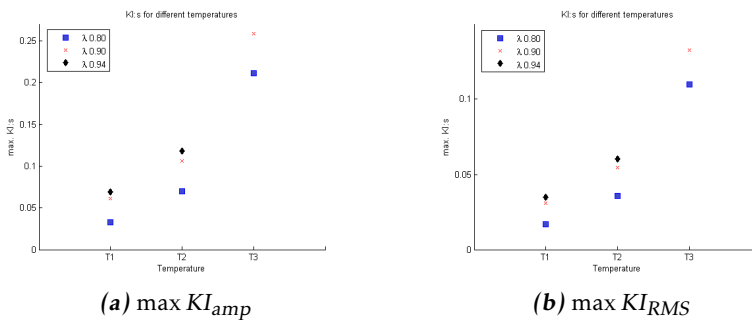
Figure 4.20: *Scatter plot for max KI:s.*

Knock intensity clearly increases with higher temperatures. The mean KI:s are nearly ten times higher when comparing the lowest temperature to the highest temperature and the mean KI:s are around 2-3 times higher when comparing the lowest temperature to the second highest. The highest temperature in table 4.9 is excluded because the combination of the lean mixture and temperature would damage the engine.

The measurements show very light to no knock with the richest mixture (λ = 0.80) together with the lowest temperature. Detectable knock levels with auxiliary knock sensors seem to start around λ = 0.90 for the lowest temperature, and at λ = 0.80 for the two higher temperatures.

4.4   Knock intensity dependency on different types of fuel

As stated in section 2.3.2, different types of fuel have a higher chance to withstand engine knock. So far the measurements have only been done using a certain test fuel. To test how the knock intensities vary with different fuels, measurements were carried out using three types of fuel.

Fuel	Description
Blend	The normal test fuel.
BlendE40	The normal test fuel diluted with 40% ethanol
Aspen	A commonly used fuel with high octane rating

Table 4.10: *Fuel types and their description.*

As the test bench can measure the correct λ value for the test fuel but not for the other fuels, the knock intensities were calculated for different power outputs from the engine instead. This was done by measuring the cylinder pressure for different power outputs, making sure that the measurements included both leaner and richer mixtures than the A/F mixture for maximum power output.
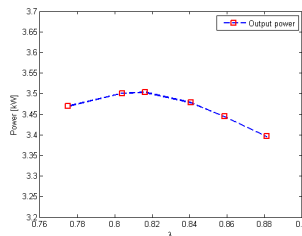
Figure 4.21: *Output power for different A/F equivalence ratios for the normal test fuel. This figure contains six different measurements.*

The KI:s from the pressure transducer were computed for each data series, and were then interpolated for a fix step away from the maximum power output to allow for an easier comparison between the fuels. The step ΔP from the maximum power output is 10 W for each fuel.

Fuel	Output power	$\overline{KI_{amp}}$	max KI_{amp}	$\overline{KI_{RMS}}$	max KI_{RMS}
Blend	$P_{max} - \Delta P$	0.0319	0.1672	0.0164	0.0870
Blend	P_{max}	0.0563	0.2399	0.0289	0.1251
Blend	$P_{max} + \Delta P$	0.0640	0.2747	0.0329	0.1420

Table 4.11: Knock intensities for test fuel "Blend". Acquired at 160 rps.

Fuel	Output power	$\overline{KI_{amp}}$	max KI_{amp}	$\overline{KI_{RMS}}$	max KI_{RMS}
BlendE40	$P_{max} - \Delta P$	0.0212	0.1032	0.0109	0.0530
BlendE40	P_{max}	0.0391	0.1627	0.0200	0.0831
BlendE40	$P_{max} + \Delta P$	0.0446	0.2198	0.0228	0.1130

Table 4.12: Knock intensities for fuel "BlendE40". Acquired at 160 rps.

Fuel	Output power	$\overline{KI_{amp}}$	max KI_{amp}	$\overline{KI_{RMS}}$	max KI_{RMS}
Aspen	$P_{max} - \Delta P$	0.0103	0.0817	0.0052	0.0419
Aspen	P_{max}	0.0142	0.0899	0.0073	0.0463
Aspen	$P_{max} + \Delta P$	0.0190	0.1876	0.0097	0.0959

Table 4.13: Knock intensities for fuel "Aspen". Acquired at 160 rps.

The highest knock intensities around P_{max} are achieved using the normal test fuel. This fuel has a very low octane rating, making it more likely to knock than the other fuels. Diluting the test fuel with ethanol lowers the knock intensities by about 40%, and also increases the maximum power output by about 100 W.

The use of Aspen results in the lowest knock intensities among the three fuels. Compared to the others it seems to only have a very light knock around maximum power output, which is also the lowest power output of the three fuels (about 10 W less than for the undiluted test fuel).

The conclusion from this experiment is that the fuel type changes the knock intensity around the maximum power output, which should be considered when using engine knock as feedback to find the optimal setting for the engine.

4.5   Knock intensity dependency on ignition timing

As stated in section 2.3.2, a knock sensor can be used to control the ignition timing of the engine. Pressure measurements at a constant engine speed and λ value with different ignition timings were done to investigate the knock level dependency on ignition.

Ignition timing	$\overline{KI_{amp}}$	$\max KI_{amp}$	$\overline{KI_{RMS}}$	$\max KI_{RMS}$
33 CAD before TDC	0.0364	0.1869	0.0188	0.0969
31 "	0.0363	0.2233	0.0188	0.1149
29 "	0.0353	0.1995	0.0181	0.1016
27 "	0.0312	0.1548	0.0160	0.0800
25 "	0.0296	0.1822	0.0151	0.0931
23 "	0.0279	0.2159	0.0142	0.1106
21 "	0.0233	0.2003	0.0118	0.1021

Table 4.14: *Knock intensities for different ignition timings. Acquired at lambda 85 and 160 rps. The mean KI:s are strictly declining for later ignition timings.*

The ignition timing affects the pressure build-up inside the cylinder. A too early ignition counteracts the piston moving upwards, and a too retarded ignition timing results in a later pressure build-up and less output torque. The knock level intensity seems to be strictly decreasing for later ignition timings when looking at the computed mean KI:s. The pressure cycle with the highest knock intensity does not decrease with later ignition timings though.

Spark advance control in the two-stroke engine could therefore be a possibility by averaging the KI:s under some crankshaft revolutions and observing the knock intensity levels. This could lead to better emissions, output torque and engine efficiency.

5

Conclusions and Future work

The final chapter presents the conclusions drawn from measurements and suggests interesting investigations for future development within the field of engine knock in small two-stroke engines.

5.1 Summary and conclusions

The main objective of the thesis has been to detect knock in a small two-stroke engine. In order to accomplish this an accelerometer has been used as an indirect sensor. The accelerometer together with a hardware filter, preferably a narrow BP filter, filtering out the first knock frequency from the accelerometer signal has turned out to be able to detect knock. However, the computed knock intensities from the accelerometer signal do not show a perfect correlation with the knock intensities from the pressure transducer. The high engine speed and the location of the accelerometer makes it hard to sense the structural vibrations from the engine knock correctly, even after the BP filter with its narrow cut-off frequency has been applied. To test closer placements to the cylinder is problematic due to the high engine block temperatures when the engine is running at WOT. To determine an adequate knock window where knock is present is important to avoid unwanted background noise in the sensor signals.

Knock intensity changes significantly along with engine temperature. It is difficult to detect any knock at all with remote located sensors when rich mixtures are combined with the lowest temperature in the temperature range of normal chainsaw operation, especially at low engine speeds.

Different types of fuel change knock intensity around maximum power output of the engine. Future engine management control could therefore benefit from taking fuel type into account to ensure optimal engine performance when including a knock sensor. Using knock detection for spark advance control to find the optimal ignition timing is also a possibility.

5.2 Future work

Other parameters that influence knock are interesting to investigate further. This could for example be engine load and speed, maybe to emulate the real operating condition when the chainsaw is used for limbing. A real chainsaw operation with the cutting equipment fully mounted would also be interesting to test.

Modern Husqvarna chainsaws come in a wide variety of models. It would be interesting to investigate the knock intensity of different engine designs.

An accelerometer with higher temperature resistance could be installed directly on the engine block without the risk of overheating the sensor. This might improve the performance of the accelerometer drastically.

Another important parameter to be investigated is weather conditions. During the measurements variations in atmospheric pressure and humidity proved to affect the knock intensity significantly.

The possibility to measure the ionic current over the spark plug as knock detection is another interesting field of research.

A

Appendix

A.1 Pressure traces for different temperatures

Below are the pressure traces corresponding to the computed mean and maximum KI:s for the three different engine temperatures.

(a) KI_{amp}, λ = 0.80 $160rps$

(b) KI_{RMS}, λ = 0.80 $160rps$

(c) KI_{amp}, λ = 0.90 $160rps$
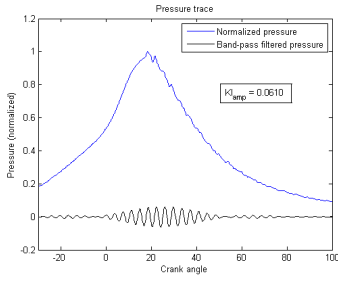
(d) KI_{RMS}, λ = 0.90 $160rps$

Figure A.1: *Cycles corresponding to the **mean** value of the computed KI:s for engine temperature T3.*
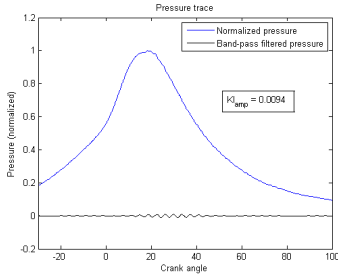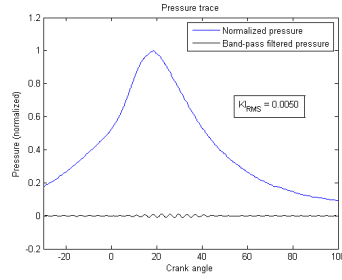
(a) KI_{amp}, $\lambda = 0.80$ $160rps$ (b) KI_{RMS}, $\lambda = 0.80$ $160rps$
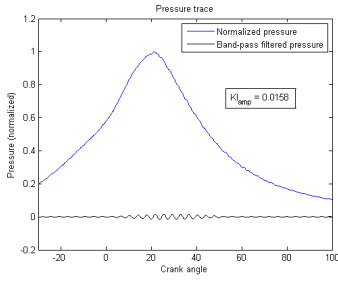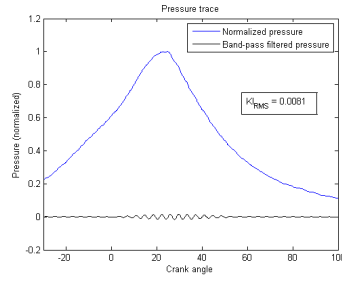
(c) KI_{amp}, $\lambda = 0.90$ $160rps$ (d) KI_{RMS}, $\lambda = 0.90$ $160rps$
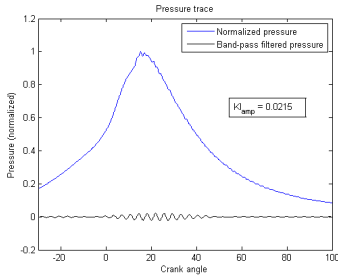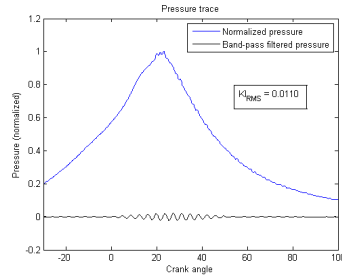
(e) KI_{amp}, $\lambda = 0.94$ $160rps$ (f) KI_{RMS}, $\lambda = 0.94$ $160rps$

Figure A.2: *Cycles corresponding to the* **mean** *value of the computed KI:s for engine temperature T2.*
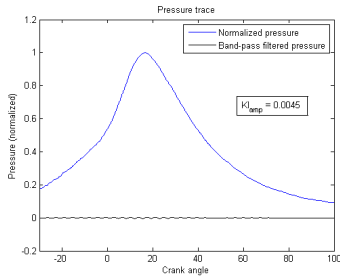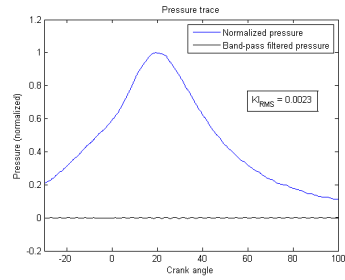
(a) KI_{amp}, $\lambda = 0.80$ 160rps   (b) KI_{RMS}, $\lambda = 0.80$ 160rps
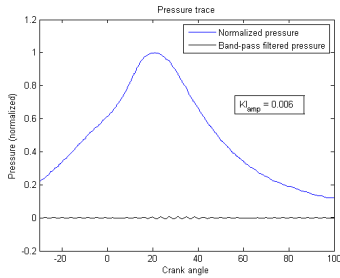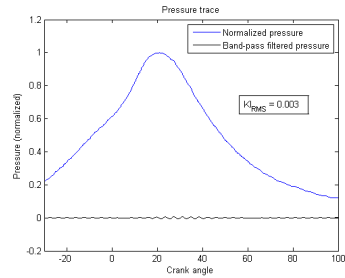
(c) KI_{amp}, $\lambda = 0.90$ 160rps   (d) KI_{RMS}, $\lambda = 0.90$ 160rps
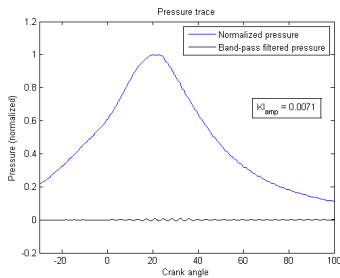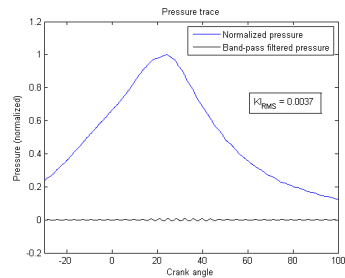
(e) KI_{amp}, $\lambda = 0.94$ 160rps   (f) KI_{RMS}, $\lambda = 0.94$ 160rps

Figure A.3: *Cycles corresponding to the* **mean** *value of the computed KI:s for engine temperature T1.*

(a) KI_{amp}, $\lambda = 0.80$ $160rps$

(b) KI_{RMS}, $\lambda = 0.80$ $160rps$

(c) KI_{amp}, $\lambda = 0.90$ $160rps$
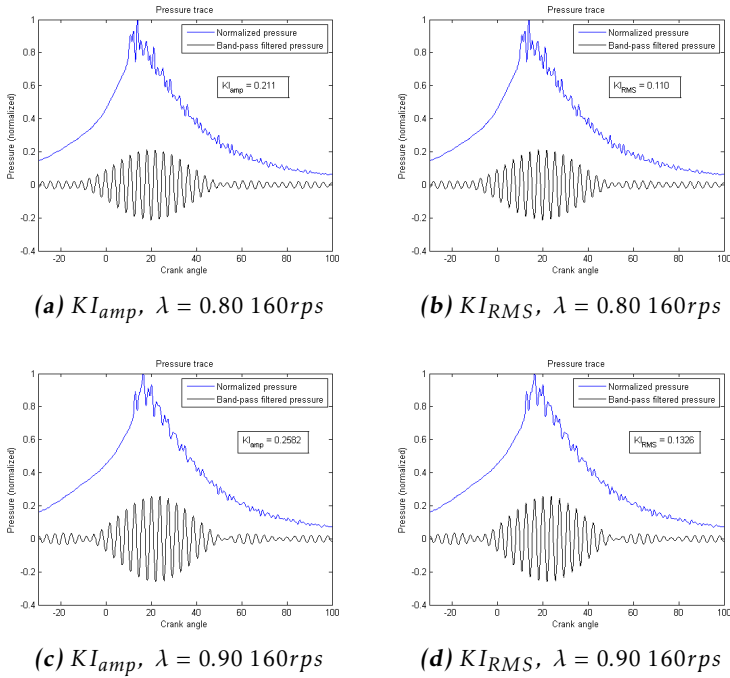
(d) KI_{RMS}, $\lambda = 0.90$ $160rps$

Figure A.4: *Cycles corresponding to the* **max** *value of the computed KI:s for engine temperature T3.*
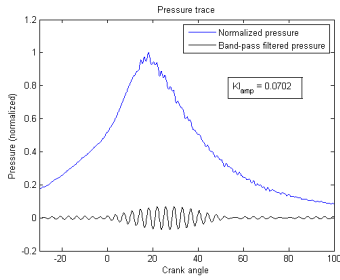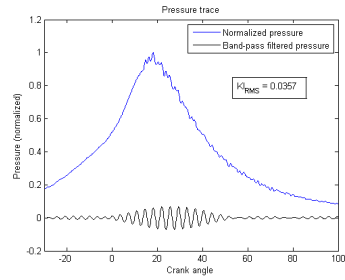
(a) KI_{amp}, $\lambda = 0.80$ 160rps
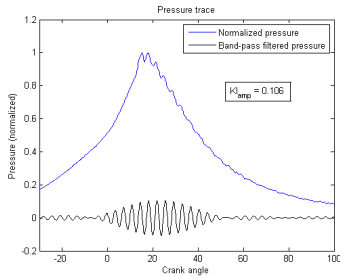
(b) KI_{RMS}, $\lambda = 0.80$ 160rps
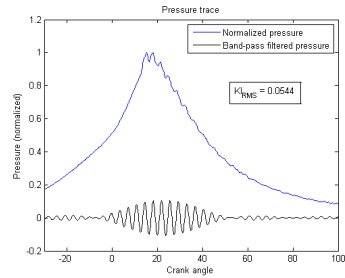
(c) KI_{amp}, $\lambda = 0.90$ 160rps
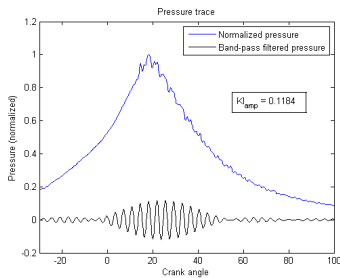
(d) KI_{RMS}, $\lambda = 0.90$ 160rps
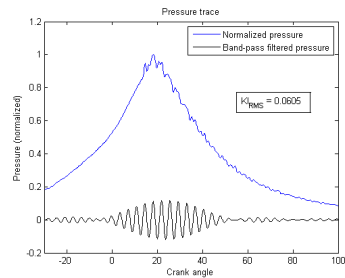
(e) KI_{amp}, $\lambda = 0.94$ 160rps

(f) KI_{RMS}, $\lambda = 0.94$ 160rps

Figure A.5: *Cycles corresponding to the **max** value of the computed KI:s for engine temperature T2.*
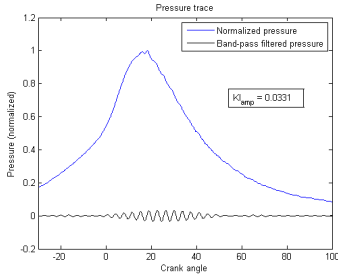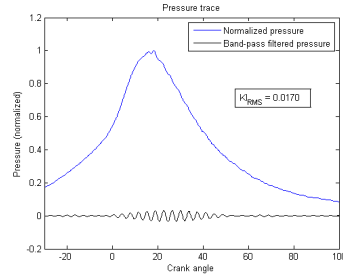
(a) KI_{amp}, $\lambda = 0.80$ $160rps$

(b) KI_{RMS}, $\lambda = 0.80$ $160rps$
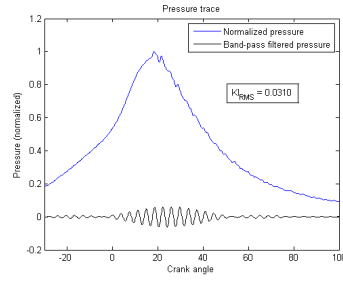
(c) KI_{amp}, $\lambda = 0.90$ $160rps$

(d) KI_{RMS}, $\lambda = 0.90$ $160rps$
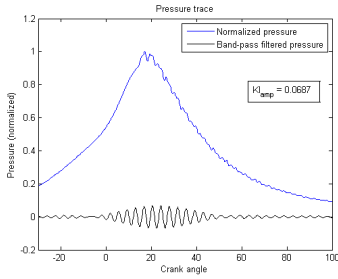
(e) KI_{amp}, $\lambda = 0.94$ $160rps$
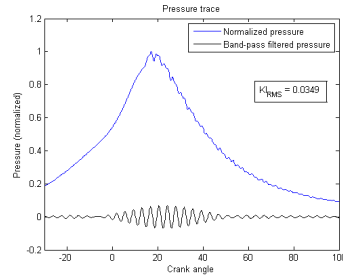
(f) KI_{RMS}, $\lambda = 0.94$ $160rps$

Figure A.6: *Cycles corresponding to the* **max** *value of the computed KI:s for engine temperature T1.*

Bibliography

[1] O. Boubai. Knock detection in automobile engines. *Instrumentation Measurement Magazine, IEEE*, 3(3):24–28, 2000. Cited on page 3.

[2] N. Harle and J.F. Bohme. Detection of knocking for spark ignition engines based on structural vibrations. In *Acoustics, Speech, and Signal Processing, IEEE International Conference on ICASSP '87.*, volume 12, pages 1744–1747, 1987. Cited on page 3.

[3] F. Molinaro, F. Castanie, and A. Denjean. Knocking recognition in engine vibration signal using the wavelet transform. In *Time-Frequency and Time-Scale Analysis, 1992., Proceedings of the IEEE-SP International Symposium*, pages 353–356, 1992. Cited on page 3.

[4] T. Jahn, F. Schuerg, and S. Kempf. Knock control on small four-two-wheeler engines. *SAE Technical Paper 2012-32-0052*, 2012. Cited on page 3.

[5] K. Schreer, K.W. Beck, S. Bernhardt, and U. Spicher. Knocking investigations in a small two-stroke SI engine. *SAE Technical Paper 2009-32-0013*, 2009. Cited on pages 3 and 4.

[6] G.P. Blair. *Design and Simulation of two-stroke Engines*. Society of Automotive Engineers, Inc., 1996. Cited on pages 6 and 7.

[7] L. Eriksson and L. Nielsen. *Modeling and Control of Engines and Drivelines*. Vehicular Systems, ISY, Linköping Institute of Technology, 2009. Cited on pages 8, 9, and 10.

[8] J.B Heywood. *Internal combustion engine fundamentals*. McGraw-Hill series in mechanical engineering. McGraw-Hill, 1988. Cited on page 9.

[9] C.S Draper. Pressure waves accompanying detonation in the internal combustion engine. *Journal of the Aeronautical Sciences*, 5, 1938. Cited on page 9.

[10] E.P. Kasseris. *Knock Limits in Spark Ignited Direct Injected Engines Using Gasoline/Ethanol Blends*. 2011. Massachusetts Institute of Technology, Department of Mechanical Engineering. Cited on pages 10 and 11.

[11] B. Rayleigh and J.W. Strutt. *The Theory of Sound*, volume 2. Macmillan and CO. LTD., 1896. Cited on page 10.

[12] Kistler Group. *High Temperature Pressure Sensor Type 6052C, Data sheet*, 2010. URL `http://www.kistler.com/uk/en/product/pressure/6052C`. Cited on page 14.

[13] PCB Group, Inc. *PCB Piezotronics Miniature Accelerometer model 352A21, Product manual*, 2002. URL `http://www.pcb.com/contentstore/docs/PCB_Corporate/Vibration/Products/Manuals/352A21.pdf`. Cited on page 14.

[14] National Instruments Corporation. *NI USB 6356 Data Acquisition Card, Data sheet*, 2012. URL `http://sine.ni.com/nips/cds/view/p/lang/en/nid/209075`. Cited on page 15.

[15] D. Dey. Characterization and rejection of noise from in-cylinder pressure traces in a diesel engine. *Electronic Theses and Dissertations*, 2012. Paper 121. Cited on page 18.

[16] F. Gustafsson, L. Ljung, and M. Millnert. *Signal Processing*. Studentlitteratur, 2010. Cited on page 24.